

Hydrothermal Synthesis of Photoluminescent Nanocarbon from Hydroxylic Acids and Amines

メタデータ	言語: eng 出版者: 公開日: 2017-10-03 キーワード (Ja): キーワード (En): 作成者: メールアドレス: 所属:
URL	http://hdl.handle.net/2297/46518

Hydrothermal Synthesis of Photoluminescent Nanocarbon from Hydroxylic Acids and Amines

Yusuke Hiejima^{1*} and Mitsuhiro Kanakubo²

¹ Department of Chemical and Materials Science, Kanazawa University, Kakuma Campus, Kanazawa 920-1192, Japan

² National Institute of Advanced Industrial Science and Technology (AIST), 4-2-1 Nigatake, Miyagino-ku, Sendai 983-8551, Japan

* Corresponding author

E-mail: hiejima@se.kanazawa-u.ac.jp

Abstract

Carbon dots (CDs) are synthesized from various pairs of hydroxylic acids and amines under hydrothermal conditions. Citric acid (CA) is paired with ethylenediamine (EDA) and the methylated analogues, and malic acid (MA), tartaric acid (TA) and mucic acid (MuA) are coupled with EDA. While the CDs from CA with EDA show strong photoluminescence, CA paired with the methyl-capped EDA derivatives gives less photoluminescent nanocarbons with a similar size of ~2 nm. The CDs from MA and TA with EDA show emission at shorter wavelengths than those from CA and MuA. The quantum yields of the CDs from CA and MA with EDA increase with the reaction time, which may be explained by modifications of the chemical structures of the CDs.

Keywords

Hydrothermal synthesis; Photoluminescence; Nanocarbon; Hydroxylic acid; Ethylenediamine

1. Introduction

Carbon dots (CDs) which are a kind of photoluminescent nanocarbon attract much attention, because of its excellent properties such as high quantum yields, high stability and low toxicity [1-11]. Moreover, CDs can be synthesized with various methods from a variety of abundant organic compounds at relatively low costs.

It has been established that the doping of nitrogen is crucial for formation of the CDs with high photoluminescence (PL) [12, 13]. A pair of citric acid (CA) and ethylenediamine (EDA) has been used as the reactants for the pyrolytic and hydrothermal syntheses [14-18], where CA and EDA are the carbon and nitrogen sources. It is noteworthy that an extremely high quantum yield of 0.94 is achieved with the pyrolysis of CA and EDA in autoclave [14]. It is also found that the molecular structures of amines drastically changes the PL properties of the CDs; EDA gives substantially higher quantum yields than other amines such as diethyl- and triethylamines [16]. Although the fact that the reactant molecules containing all of -OH, -COOH and -NH₂ groups give the CDs with high PL has been pointed out [15], the relation between the structures of the reactant molecules and the physicochemical properties of the CDs is still unclear.

In this work, we have conducted hydrothermal syntheses of CDs from various pairs of hydroxylic acids and amines. The effects of the molecular structures of the acids and amines on the physicochemical properties of the CDs are discussed.

2. Experimental

CA was purchased from Aldrich. Malic acid (MA), tartaric acid (TA), mucic acid (MuA), anhydrous EDA, *N,N*-dimethylethylenediamine (DMEDA) and *N,N,N',N'*-tetramethylethylenediamine (TMEDA) were purchased from Tokyo Chemical Industries. These reactant reagents were used as received. The chemical structures of these hydroxylic acid and amines are shown in Figure 1. The aqueous solutions of the hydroxylic acids and amines were prepared. The concentration of hydroxylic acids was set at 0.5 M, except for MuA (0.1 M) which has lower solubility in water than other hydroxylic acids. The molar ratio of amines to hydroxylic acids was 2.0 for EDA, and 1.0 for DMEDA and TMEDA. A SUS316 tube-shaped batch reactor with the sample volume of ~10 mL was used for the hydrothermal synthesis of CDs. The sample solution was sealed in the reactor, where about 95 % of the reactor volume was filled with the sample solution to avoid biphasic conditions under the liquid-vapor equilibrium at the reaction

temperature. The reactors were placed in an oven with a 2 kW heater (Watlow), and heated at 200 °C for 1-4 h. After the reaction time, the reactors were taken out of the furnace, followed by cooling at room temperature. The temporal changes of the temperature were monitored by a thermocouple immersed in the solution, and the heating and cooling rates of the sample solution were ~30 and ~-5 °C/min, respectively. The recovered solution was dialyzed in a cellulose ester membrane (Spectra/Por, MWCO=100-500) for one day to remove compounds with low molecular weights. The obtained solution was filtered with a membrane with a pore size of 0.22 μm to remove solid byproducts. The yield of the CDs was calculated by dividing the vacuum-dried weight of the CDs by a sum of the weight of reactants (hydroxylic acid and amine).

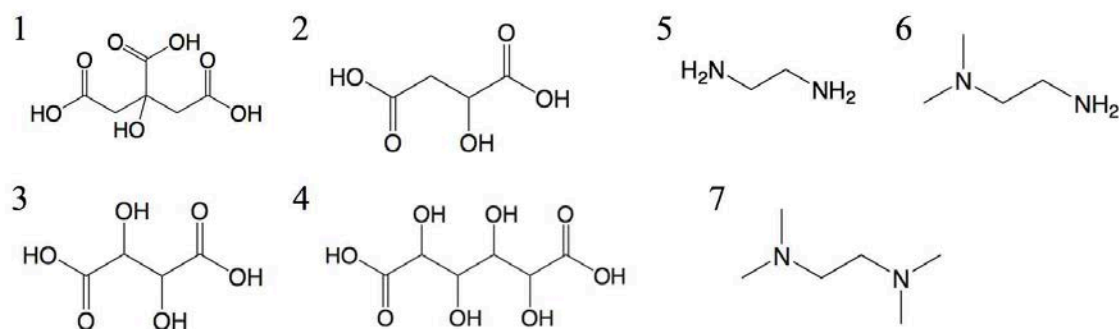


Fig. 1 Chemical structures of hydroxylic acids (1. citric acid (CA), 2. malic acid (MA), 3. tartaric acid (TA) and 4. mucic acid (MuA)) and amines (5. ethylenediamine (EDA), 6. *N,N*-dimethylethylenediamine (DMEDA) and 7. *N,N,N',N'*-tetramethylethylenediamine (TMEDA)).

For the spectroscopic analyses, each aqueous solution of the CDs was diluted by 10^2 times. The absorption spectra of the CDs solution were measured by a UV-visible spectrophotometer (Jasco, V-550). The PL spectra of the aqueous solutions of the CDs were collected by a fluorescence spectrophotometer (Hitachi High-Technologies, F-2700). The quantum yield of the CDs was determined by the comparative method [19]. The quinine sulfate solution in 0.5 M H_2SO_4 was used as the reference [20]. A drop of aqueous solution of the CDs was dried on a TEM grid which was pretreated by plasma in vacuum to make the surface hydrophilic. The TEM images of the CDs were obtained with a transmission electron microscope (Hitachi High-Technologies, H-7650). The 1H and ^{13}C NMR spectra of the CDs dissolved in D_2O were measured with spectrometers (JEOL, ECA-600 and ECS-400).

3. Results and discussion

As shown in Table 1, the yield of the CDs from the hydroxylic acids with EDA increases with increasing the reaction time, except for those from MuA. The increasing rate becomes gradual at the longer reaction time, suggesting that the formation of CDs takes place in the early stage. The decrease of yield for MuA at the longer reaction time may be due to formation of solid byproducts which were not observed for other hydroxylic acids. The TEM images and the size distributions of the CDs from CA with EDA are shown in Figure 2. Nanoparticles with the diameters of 1-5 nm are observed. The average size of nanoparticles appreciably decreases with increasing the reaction time. The decrease of the size of the CDs might lead to narrower distribution, because the experimental lower limit of the size distribution is close to the pore size of the dialyzing membrane (slightly smaller than 1 nm). According to the proposed mechanism of CDs formation [17, 18, 21], polymerization of CA and EDA is considered to be followed by the formation of CDs accompanied by various changes of the chemical structures. Then, the slight shrinkage of the CDs may be caused by detachment of small molecules such as dehydration from the CDs.

Table 1 Reaction conditions and yields, average diameters and quantum yields of CDs.

Run	Hydroxylic acid	Amine	Reaction time [h]	Yield of CDs [wt.%]	Average diameter [nm]	Φ_{366} [-] ^{*1}
1	CA	EDA	1	17.6	2.7	0.11
2	CA	EDA	2	20.5	1.9	0.23
3	CA	EDA	4	28.7	1.8	0.29
4	CA	DMEDA	2	24.3	2.0	0.11
5	CA	TMEDA	2	16.8	2.0	- ^{*2}
6	MA	EDA	1	12.5	2.0	2.8×10^{-2}
7	MA	EDA	2	14.5	2.1	4.5×10^{-2}
8	MA	EDA	4	15.6	2.0	0.11
9	TA	EDA	1	12.7	2.1	2.9×10^{-2}
10	TA	EDA	2	16.7	2.2	3.1×10^{-2}
11	TA	EDA	4	17.4	2.0	2.9×10^{-2}

12	MuA	EDA	1	34.3	1.9	2.2×10^{-2}
13	MuA	EDA	2	19.5	2.1	6.2×10^{-2}
14	MuA	EDA	4	9.1	1.9	7.0×10^{-2}

*¹ Quantum yield at 366 nm excitation.

*² No PL emission is observed.

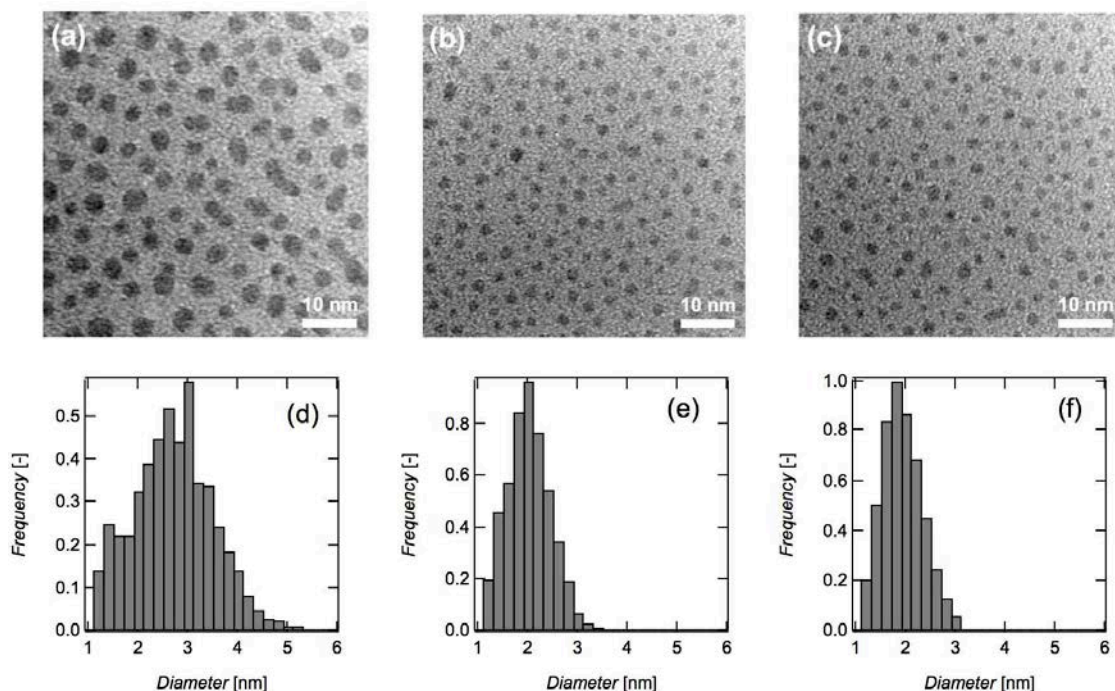


Fig. 2 TEM images and size distributions of CDs from CA with EDA at reaction times of (a, d) 1 h (b, e) 2 h and (c, f) 4 h.

In Figure 3, the absorption spectra of the CDs from CA are shown. The absorption band in the UV region at ~ 340 nm assigned to the $n-\pi^*$ transition [14, 22] sharply increases with the reaction time due to the formation of CDs. The contour plots of PL intensities of the CDs from CA with EDA are shown in Figure 4. The corresponding emission and excitation spectra which are obtained as the slice plots of Figure 4 are shown in S-1 in Supporting Information. The CDs at the reaction time of 1 h shows strong blue emission centered at ~ 450 nm under UV excitation at ~ 350 nm. For the CDs at longer reaction times, the blue emission becomes weaker, and the range of the emission and excitation wavelengths spread toward longer wavelength, resulting in wavelength dependent PL emission as reported in the previous works [15, 16, 21, 23]. The red shifts of the emission and excitation spectra are in accordance with the increase of the absorption tail in Figure 3. The spectral changes of the PL emission suggests that the formation

of carbogenic core which is considered to give emission at longer wavelengths [21]. Because careful fractionation of the CDs by their different surface polarities gives several distinct absorption bands in visible light region [24], the red shift may be caused by the surface modification of the CDs.

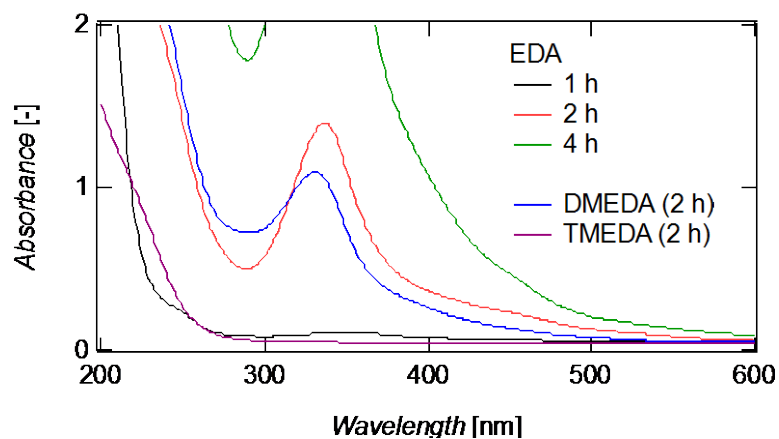


Fig. 3 Absorption spectra of CDs from CA with EDA, DMEDA and TMEDA. The reaction times are also shown.

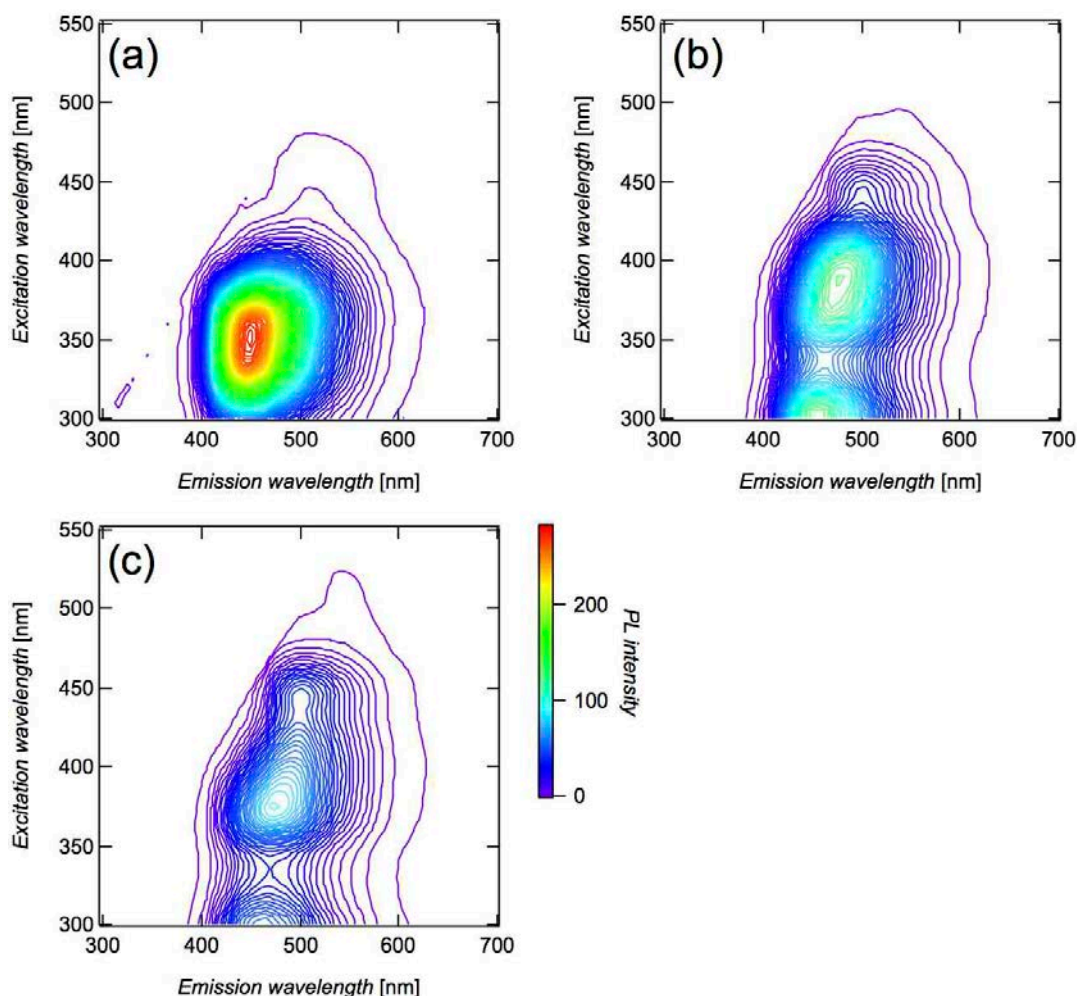


Fig. 4 Contour plots of PL intensities for CDs from CA with EDA. The reaction time is (a) 1 h, (b) 2 h and (c) 4 h.

For the methylated EDAs (DMEDA and TMEDA), the intensity of the absorption band at ~ 330 nm becomes substantially smaller than those from EDA as shown in Figure 3. However, the formation of nanoparticle with the size of about 2.0 nm is confirmed by the TEM observation (see S-2 in Supporting Information). Moreover, the yield of the nanocarbon is only slightly smaller than those from EDA as shown in Table 1. According to the proposed mechanism of formation [18], the polymerization and the following nanoparticle formation are expected to be suppressed by using the capped EDA. However, in the present study, similar nanocarbons are formed without drastic decrease of the yield, whereas the PL is quite suppressed. Then, it is suggested that the formation of fluorophore is suppressed by capping of the amino groups.

The absorption spectra of the CDs from MA, TA and MuA are shown in Figure 5. The

intensity of the absorption bands in the UV region increases with the reaction time, suggesting formation of the CDs. For the CDs from MA, TA and MuA, CDs with the average size of about 2.0 nm are also confirmed by the TEM observation (see S-3 in Supporting Information). The size distribution of the CDs from MA, TA and MuA shows no appreciable dependence on the reaction time, implying that the chemical modifications to form the fluorophores in the CDs are less effective in these systems compared to CA.

The contour plots of the PL intensity of the CDs from MA, TA and MuA are shown in Figure 6 (See also the corresponding emission and excitation spectra shown as S-4 in Supporting Information). The CDs from MA and TA show emission at ~400 nm under the excitation at 300-350 nm, and the emission intensity monotonously decreases at longer excitation wavelengths. The PL emission of the CDs from MuA is located at ~400nm, accompanied by the emission at longer wavelength (~460 nm emission under ~380 nm excitation), which is similar to that observed for the CDs from CA with EDA.

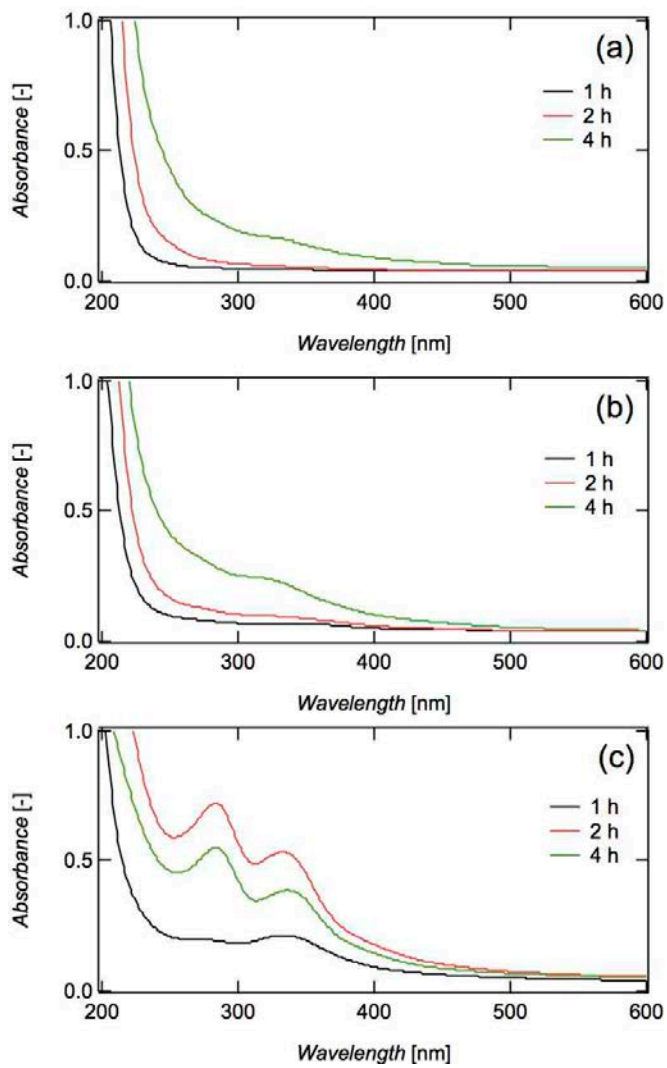


Fig. 5 Absorption spectra of CDs from (a) MA, (b) TA and (c) MuA. The reaction times are also shown.

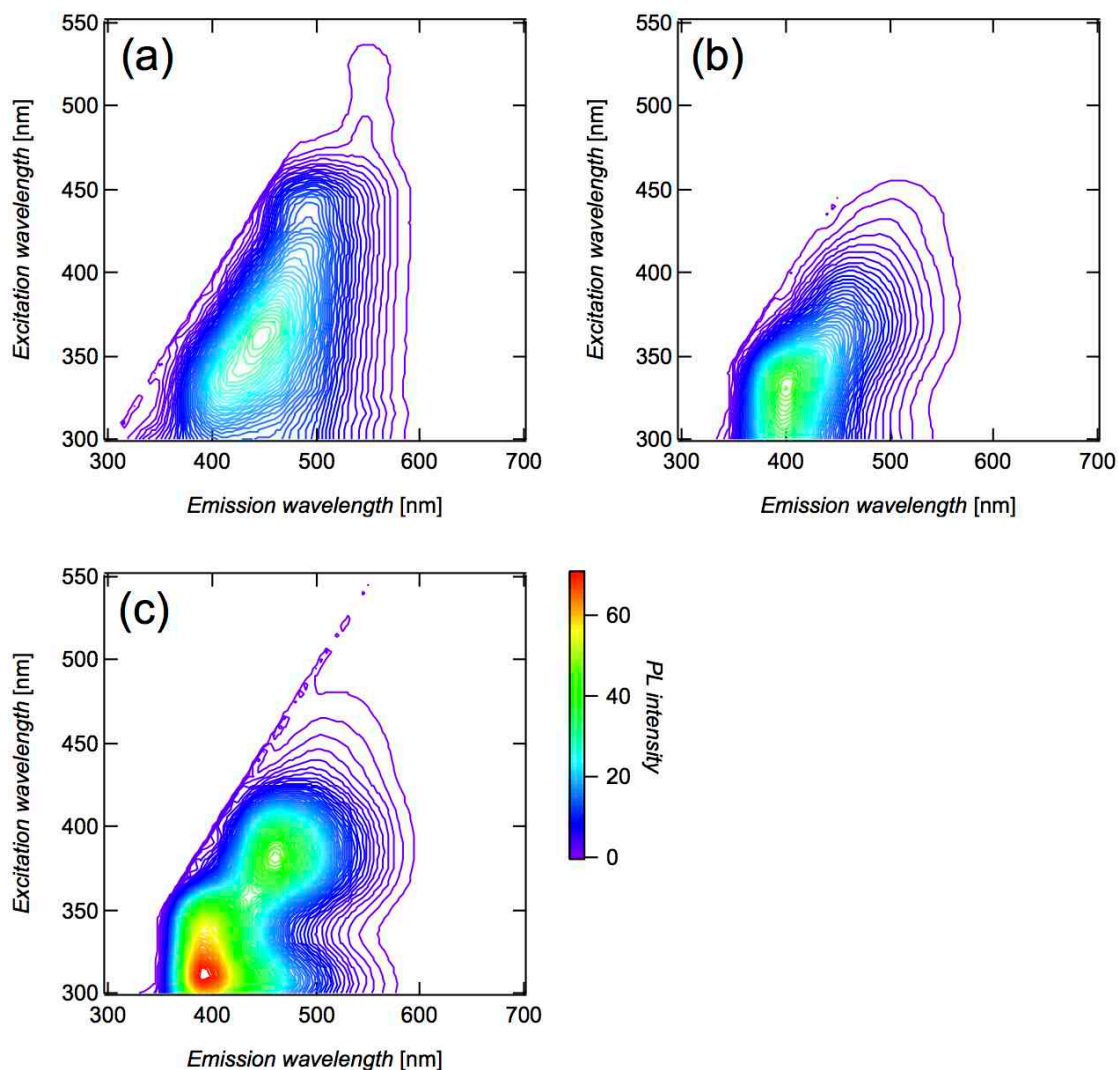


Fig. 6 Contour plots of PL intensities for CDs from (a) MA, (b) TA and (c) MuA at a reaction time of 4 h.

The quantum yield (Φ_{366}) of the CDs from CA with EDA sharply increases with the reaction time as shown in Table 1. The quantum yield of the CDs from MA also increases with the reaction time, while that from TA remains low even for the longer reaction time. The reaction time dependence of the quantum yield may be explained by the gradual change of the chemical structure of the CDs as follows. The results of the elemental analyses of the CDs from CA and MA are shown in Table 2. The hydrogen and oxygen contents appreciably decrease with the reaction time, which may be explained by the dehydration of the CDs during heating. The modification of the chemical structure is also evidenced by the NMR spectra in Figures 7 and 8. The growth of the signals due to the aromatic and olefinic protons indicates the formation of sp^2

carbons. The CH₂ protons in CA and MA (δ ~2.5 ppm) and in EDA (δ =3.2 ppm) seem to be converted to the CH₂ and CH protons observed as the complicated signals at ~3 ppm, which is consistent with the spectral changes of the ¹³C NMR spectra at ~40 ppm. The FT-IR spectra of the CDs (S-5 in Supporting Information) indicate the persistence of the OH group (3340 cm⁻¹) which is responsible for hydrophilicity of the CDs. A peak due to the C=O stretching mode is observed at 1710 cm⁻¹, and the spectral shape in the N-H bending region (~1550 cm⁻¹ [22]) shows appreciable change with the reaction time, suggesting structural modification in the vicinity of the amino group. Although the reaction mechanism is not clear, these spectral changes may be caused by various reactions such as amidation and dehydration during the inclusion of N atoms into the CDs.

Table 2 Elemental analyses of CDs synthesized from hydroxylic acids and EDA.

Hydroxylic acid	Reaction time [h]	H [wt.%]	C [wt.%]	N [wt.%]	O [wt.%] [*]
CA	1	5.4	38.9	7.8	47.9
CA	2	5.0	43.3	8.2	43.5
CA	4	5.1	48.6	10.1	36.2
MA	1	6.6	35.3	11.4	46.7
MA	2	6.3	38.1	11.8	43.8
MA	4	6.1	39.9	12.5	41.5

^{*} Determined from the residual.

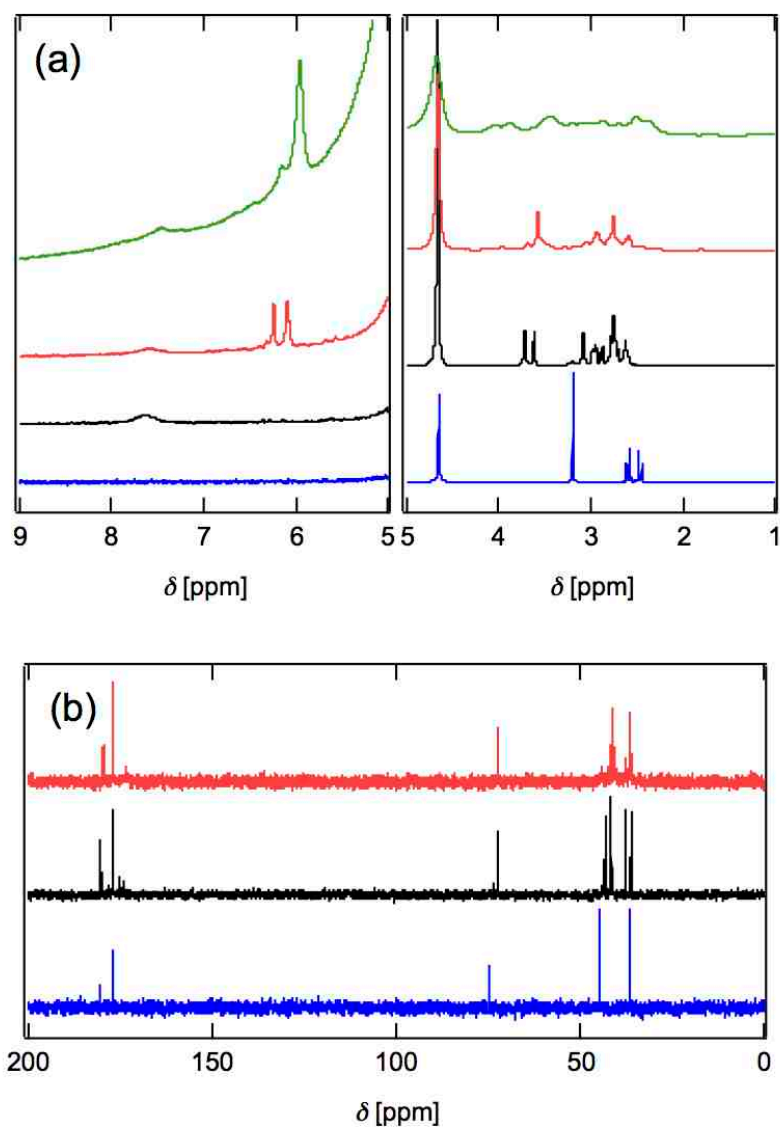


Fig. 7 (a) ^1H and (b) ^{13}C NMR spectra of CDs from CA with EDA at reaction times of 1 h (black), 2 h (red) and 4 h (green). The spectra of the salt of CA and EDA are shown by the blue lines.

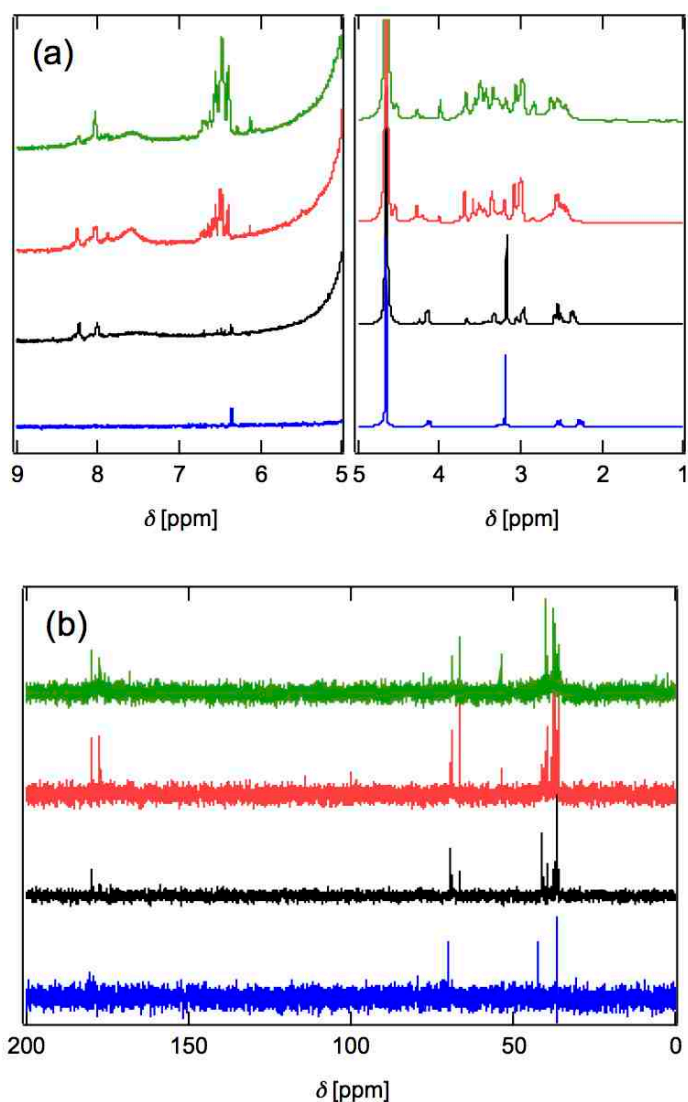


Fig. 8 (a) ^1H and (b) ^{13}C NMR spectra of CDs from MA at reaction times of 1 h (black), 2 h (red) and 4 h (green). The spectra of the salt of MA and EDA are shown by the blue lines.

4. Conclusion

Hydrothermal synthesis of CDs from various hydroxylic acids and amines was conducted. The quantum yield of the CDs from CA with EDA increases with the reaction time, while the addition of the methylated EDA derivatives instead of EDA gives less or no photoluminescent nanocarbons with the similar size without lowering the yields. Other hydroxylic acids with EDA give the CDs, though the quantum yields are lower than those from CA with EDA. In spite of the variation of the chemical structures of the reactant molecules, similar nanocarbons are obtained without affecting the yields, suggesting that the modifications to form the fluorophores

in the CDs during heating are responsible for the PL properties of CDs.

Acknowledgment

YH is thankful to Prof. Koh-hei Nitta at Kanazawa University for his continuous encouragement for this work. This work was financially supported by Adaptable and Seamless Technology Transfer Program (A-STEP) of Japan Science and Technology Agency (JST). The TEM images were measured at Japan Advanced Institute of Science and Technology (JAIST), supported by Nanotechnology Platform Program of the Ministry of Education, Culture, Sports, Science and Technology (MEXT), Japan.

References

1. Baker, S., Baker, G.: Luminescent Carbon Nanodots: Emergent Nanolights. *Angew Chem Int Ed.* 49, 6726–6744 (2010).
2. Cao, L., Meziani, M.J., Sahu, S., Sun, Y.-P.: Photoluminescence properties of graphene versus other carbon nanomaterials. *Acc Chem Res.* 46, 171–180 (2013).
3. Li, H., Kang, Z., Liu, Y., Lee, S.-T.: Carbon nanodots: synthesis, properties and applications. *J Mater Chem.* 22, 24230–24253 (2012).
4. Hola, K., Zhang, Y., Wang, Y., Giannelis, E.P., Zboril, R., Rogach, A.L.: Carbon dots—Emerging light emitters for bioimaging, cancer therapy and optoelectronics. *Nano Today.* 9, 590–603 (2014).
5. Miao, P., Han, K., Tang, Y., Wang, B., Lin, T., Cheng, W.: Recent advances in carbon nanodots: synthesis, properties and biomedical applications. *Nanoscale.* 7, 1586–1595 (2015).
6. Zhu, S., Song, Y., Zhao, X., Shao, J., Zhang, J., Yang, B.: The photoluminescence mechanism in carbon dots (graphene quantum dots, carbon nanodots, and polymer dots): current state and future perspective. *Nano Res.* 8, 355–381 (2015).
7. Zhao, A., Chen, Z., Zhao, C., Gao, N., Ren, J., Qu, X.: Recent advances in bioapplications of C-dots. *Carbon.* 85, 309–327 (2015).
8. Kargbo, O., Jin, Y., Ding, S.-N.: Recent Advances in Luminescent Carbon Dots. *Curr Anal Chem.* 11, 4–21 (2015).
9. Zheng, X.T., Ananthanarayanan, A., Luo, K.Q., Chen, P.: Glowing Graphene Quantum Dots and Carbon Dots: Properties, Syntheses, and Biological Applications. *Small.* 11, 1620–1636 (2015).
10. Lim, S.Y., Shen, W., Gao, Z.: Carbon quantum dots and their applications. *Chem Soc Rev.* 44, 362–381 (2015).
11. Himaja, A.L., Karthik, P.S., Singh, S.P.: Carbon Dots: The Newest Member of the Carbon Nanomaterials Family. *Chem Record.* 15, 595–615 (2015).
12. Li, W., Zhang, Z., Kong, B., Feng, S., Wang, J., Wang, L., Yang, J., Zhang, F., Wu, P., Zhao, D.: Simple and Green Synthesis of Nitrogen-Doped Photoluminescent Carbonaceous Nanospheres for Bioimaging. *Angew Chem Int Ed.* 52, 8151–8155 (2013).

13. Dong, Y., Pang, H., Yang, H.B., Guo, C., Shao, J., Chi, Y., Li, C.M., Yu, T.: Carbon-Based Dots Co-doped with Nitrogen and Sulfur for High Quantum Yield and Excitation-Independent Emission. *Angew Chem Int Ed.* 52, 7800–7804 (2013).
14. Qu, D., Zheng, M., Zhang, L., Zhao, H., Xie, Z., Jing, X., Haddad, R.E., Fan, H., Sun, Z.: Formation mechanism and optimization of highly luminescent N-doped graphene quantum dots. *Sci Rep.* 4, (2014).
15. Zhu, S., Meng, Q., Wang, L., Zhang, J., Song, Y., Jin, H., Zhang, K., Sun, H., Wang, H., Yang, B.: Highly photoluminescent carbon dots for multicolor patterning, sensors, and bioimaging. *Angew Chem Int Ed.* 52, 3953–3957 (2013).
16. Zhai, X., Zhang, P., Liu, C., Bai, T., Li, W., Dai, L., Liu, W.: Highly luminescent carbon nanodots by microwave-assisted pyrolysis. *Chem Commun.* 48, 7955–7957 (2012).
17. Wang, J., Zhang, P., Huang, C., Liu, G., Leung, K.C.-F., Wang, Y.X.J.: High Performance Photoluminescent Carbon Dots for In Vitro and In Vivo Bioimaging: Effect of Nitrogen Doping Ratios. *Langmuir.* (2015).
18. Song, Y., Zhu, S., Zhang, S., Fu, Y., Wang, L., Zhao, X., Yang, B.: Investigation from chemical structure to photoluminescent mechanism: a type of carbon dots from the pyrolysis of citric acid and an amine. *J Mater Chem C.* 3, 5976–5984 (2015).
19. Lakowicz, J.R.: *Principles of Fluorescence Spectroscopy.* Springer (2009).
20. Brouwer, A.M.: Standards for photoluminescence quantum yield measurements in solution (IUPAC Technical Report). *Pure Appl Chem.* 83, 2213–2228 (2011).
21. Krysmann, M.J., Kellarakis, A., Dallas, P., Giannelis, E.P.: Formation mechanism of carbogenic nanoparticles with dual photoluminescence emission. *J Am Chem Soc.* 134, 747–750 (2012).
22. Dhenadhayalan, N., Lin K.-C., Suresh, R., Ramamurthy, P.: Unravelling the Multiple Emissive States in Citric-Acid-Derived Carbon Dots. *J Phys Chem C.* 120, 1252–1261 (2016).
23. Bourlinos, A.B., Stassinopoulos, A., Angelos, D., Zboril, R., Georgakilas, V., Giannelis, E.P.: Photoluminescent carbogenic dots. *Chem Mater.* 20, 4539–4541 (2008).
24. Ding, H., Yu, S.-B., Wei, J.-S., Xiong, H.-M.: Full-Color Light-Emitting Carbon Dots with a Surface-State-Controlled Luminescence Mechanism. *ACS Nano.* 10, 484–491 (2016).

Graphical abstract

